A New Variable-Speed Wind Energy Conversion System Using Permanent-Magnet Synchronous Generator and Z-Source Inverter

Seyed Mohammad Dehghan, *Student Member, IEEE*, Mustafa Mohamadian, *Member, IEEE*, and Ali Yazdian Varjani, *Member, IEEE*

***Abstract*—With the growth of wind energy conversion systems (WECSs), various technologies are developed for them. Permanent-magnet synchronous generators (PMSGs) are used by these technologies due to special characteristics of PMSGs such as low weight and volume, high performance, and the elimination of the gearbox. In this paper, a new variable-speed WECS with a PMSG and Z-source inverter is proposed. Characteristics of Z-source inverter are used for maximum power tracking control and delivering power to the grid, simultaneously. Two control methods are proposed for delivering power to the grid: Capacitor voltage control and dc-link voltage control. Operation of system with these methods is compared from the viewpoint of power quality and total switching device power (TSDP). In addition, TSDP, current ripple of inductor, performance, and total harmonic distortion of grid current of proposed system is compared with traditional wind energy system with a boost converter.**

***Index Terms*—Maximum power point tracking (MPPT) control, permanent-magnet synchronous generator (PMSG), wind energy conversion system (WECS), Z-source inverter.**

I. Introduction

WIND TURBINES usage as sources of energy has increased significantly in the world. With growing application of wind energy conversion systems (WECSs), various technologies are developed for them. With numerous advantages, permanent-magnet synchronous generator (PMSG) generation system represents an important trend in development of wind power applications [1]–[6]. Extracting maximum power from wind and feeding the grid with high-quality electricity are two main objectives for WECSs. To realize these objectives, the ac–dc–ac converter is one of the best topology for WECSs [2]–[6]. Fig. 1 shows a conventional configuration of ac–dc–ac topology for PMSG. This configuration includes diode rectifier, boost dc–dc converter and three-phase inverter. In this topology, boost converter is controlled for maximum power point tracking (MPPT) and inverter is controlled to deliver high-quality power to the grid [2]–[4].

The Z-source inverters have been reported recently as a competitive alternative to existing inverter topologies with many inherent advantages such as voltage boost [7]. This inverter facilitates voltage boost capability with the turning ON of both switches in the same inverter phase leg (shoot-through state).

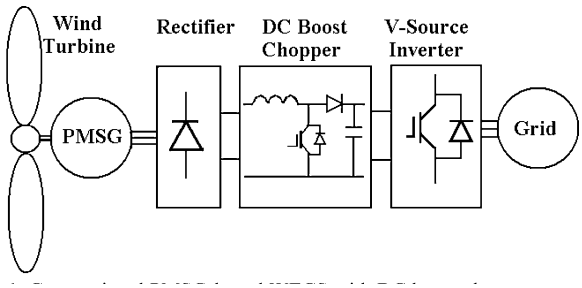

Fig. 1. Conventional PMSG-based WECS with dc boost chopper.

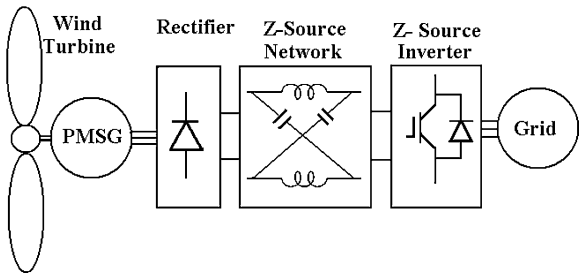

Fig. 2. Proposed PMSG-based WECS with Z-source inverter.

In this paper, a new PMSG-based WECS with Z-source inverter is proposed. The proposed topology is shown in Fig. 2. With this topology, boost converter is omitted without any change in the objectives of WECS. Moreover, reliability of the system is greatly improved, because the short circuit across any phase leg of inverter is allowed. Also, in this configuration, inverter output power distortion is reduced, since there is no need to phase leg dead time.

Section II of this paper introduces Z-source inverter and describes operation of rectifier feeding the Z-source inverter. Then, power delivery and MPPT control of system are explained. Finally, simulation results are presented to verify the performance of the proposed system.

II. Z-Source Inverter

The Z-source inverter is shown in Fig. 3. This inverter has an impedance network on its dc side, which connects the source to the inverter. The impedance network is composed of two inductors and two capacitors. The conventional voltage source inverters have six active vectors and two zero vectors. However,

Manuscript received June 3, 2008; revised September 21, 2008. First published June 10, 2009; current version published August 21, 2009. Paper no. TEC-00197-2008.

The authors are with the Department of Electrical and Computer Engineering, Tarbiat Modares University, Tehran 1411713116, Iran (e-mail: dehghansm@modares.ac.ir; mohamadian@modares.ac.ir; yazdian.modares.ac.ir).

Digital Object Identifier 10.1109/TEC.2009.2016022

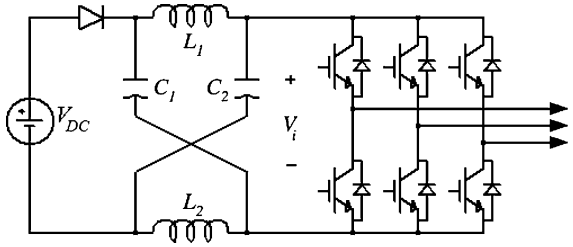

Fig. 3. Voltage-type Z-source inverter.

the Z-source inverter has one extra zero vector (state) for boosting voltage that is called shoot-through vector. In this state, load terminals are shorted through both the upper and lower devices of any one phase leg, any two phase legs, or all three phase legs.

As described in [7], the voltage of dc link can be expressed as

$$V_i = BV_{\rm dc} \tag{1}$$

where $V_{\rm dc}$ is the source voltage and B is the boost factor that is determined by

$$B = \frac{1}{1 - 2(T_o/T)} \tag{2}$$

where T_o is the shoot-through time interval over a switching cycle T. The output peak phase voltage $V_{\rm ac}$ is

$$V_{\rm ac} = MB\frac{V_{\rm dc}}{2} \tag{3}$$

where M is the modulation index. The capacitors voltage can expressed as

$$V_C = V_{C1} = V_{C2} = \frac{T_1}{T_1 - T_o}V_{\rm dc} \tag{4}$$

where

$$T_1 = T - T_o. \tag{5}$$

Relation between V_i and V_C can be written as

$$V_i = 2V_C - V_{\rm dc}. \tag{6}$$

And current ripple of inductors can be calculated by

$$\Delta I = \frac{T_1 T_o}{T_1 - T_o}\frac{V_{\rm dc}}{L}. \tag{7}$$

Fig. 4 illustrates the simple PWM control method for Z-source inverter. This method employs two extra straight lines as shoot-through signals, V_{SC} and $-V_{SC}$. When the career signal is greater than V_{SC} or it is smaller than $-V_{SC}$, a shoot-through vector is created by inverter. The value of V_{SC} is calculated by

$$V_{SC} = \frac{T_1}{T}. \tag{8}$$

In the proposed WECS, a diode rectifier bridge with input capacitors (C_a, C_b, and C_c) serves as the dc source feeding the Z-source inverter. This configuration is shown in Fig. 5. The input capacitors suppress voltage surge that may occur due to the line inductance during diode commutation and shoot-through mode of the inverter [9].

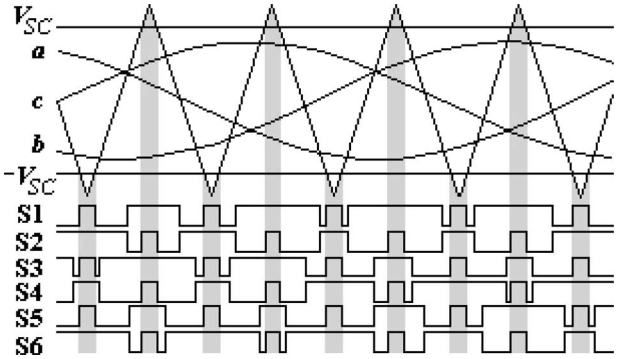

Fig. 4. PWM control method for Z-source inverter.

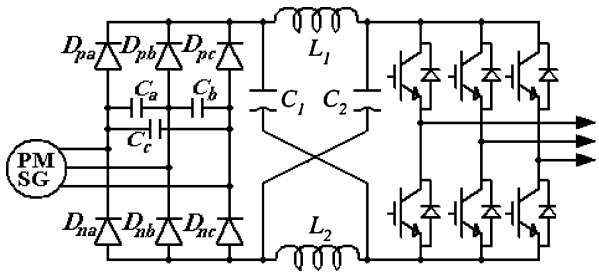

Fig. 5. Z-source inverter fed with a diode rectifier bridge.

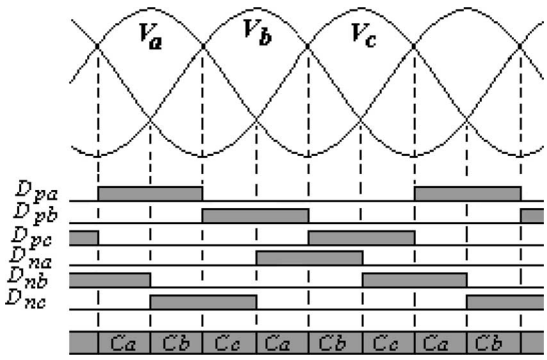

Fig. 6. Six possible conduction intervals for the rectifier.

At any instant of time, only two phases that have the largest potential difference may conduct, carrying current from the PMSG side to the impedance network side. Fig. 6 shows six possible states during each cycle. In any state, one of upper diodes, one of lower diodes, and the corresponding capacitor are active. For example, when the potential difference between phases "a" and "b" is the largest, diodes D_{pa} and D_{nb} conduct in series with capacitor C_a, as shown in Fig. 7.

In each conduction interval, inverter operates in two modes. In mode 1, the inverter is operating in the shoot-through state. In this mode, the diodes (D_{pa} and D_{nb}) are off, and the dc link is separated from the ac line. Fig. 8 shows the equivalent circuit in this mode. In mode 2, the inverter is applying one of the six active vectors or two zero vectors, thus acting as a current source viewed from the Z-source circuit with diodes (D_{pa} and D_{nb}) being on. Fig. 9 shows the equivalent circuit in this mode. The load current i_i is zero during zero vectors.

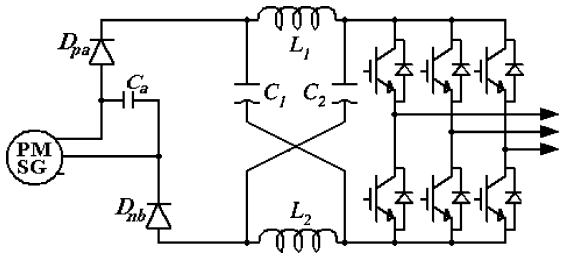

Fig. 7. Equivalent circuit when the potential difference between phases "a" and "b" is the largest.

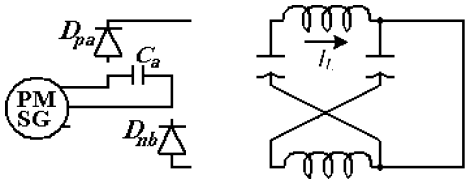

Fig. 8. Equivalent circuit of the Z-source inverter in mode 1.

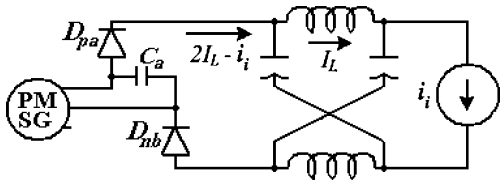

Fig. 9. Equivalent circuit of the Z-source inverter in mode 2.

III. Control System

The structure of the control system is shown in Fig. 10. The control system is composed of two parts: 1) control of power delivered to the grid and 2) MPPT.

A. Control of Power Delivered to the Grid

The power equations in the synchronous reference frame are given by [6]

$$P = \frac{3}{2}(v_d i_d + v_q i_q) \tag{9}$$

$$Q = \frac{3}{2}(v_q i_d - v_d i_q) \tag{10}$$

where P and Q are active and reactive power, respectively, v is grid voltage, and i is the current to the grid. The subscripts "d" and "q" stand for direct and quadrature components, respectively. If the reference frame is oriented along the grid voltage, v_q will be equal to zero. Then, active and reactive power may be expressed as

$$P = \frac{3}{2} v_d i_d \tag{11}$$

$$Q = -\frac{3}{2} v_d i_q. \tag{12}$$

According to earlier equations, active and reactive power control can be achieved by controlling direct and quadrature current components, respectively.

Two control paths are used to control these currents. In the first path, with given reactive power, the q-axis current reference is set. To obtain unit power factor, the q-axis current reference should be set to 0. In the second path, an outer capacitor voltage control loop is used to set the d-axis current reference for active power control. This assures that all the power coming from the rectifier is transferred to the grid. For this control, two methods are proposed: 1) capacitor voltage (V_C) control and 2) dc-link voltage (V_i) control.

In the first control method (control mode 1 in Fig. 10), capacitor voltage is kept constant at reference value. In the control loop, when shoot-through time changes, $V_{\rm dc}$ and V_i will change. However, in other method (control mode 2 in Fig. 10), a reference value is set for dc-link voltage (V_i). In this method, with changing shoot-through time, $V_{\rm dc}$ and V_C will change. The input voltage of inverter is zero in shoot through state, which makes V_i a difficult variable to control. Consequently, (6) is used to control V_i indirectly by controlling V_C. In Section IV, operation of system using these methods will be compared.

B. Maximum Power Point Tracking

The mechanical power delivered by a wind turbine is expressed as

$$P_m = \frac{1}{2}\rho A c_p v_m^3 \tag{13}$$

where ρ is the air density, A is the area swept out by the turbine blades, v_w is the wind velocity, and c_p is the power coefficient defined as the ratio of turbine power to wind power and depends on the aerodynamic characteristics of blades. Fig. 11 represents the relation between generator speed and output power according to wind speed change. It is observed that the maximum power output occurs at different generator speeds for different wind velocities.

The steady-state-induced voltage and torque equations of PMSG are given by

$$T = K_t I_a \tag{14}$$

$$E = K_e \omega \tag{15}$$

where ω is rotor speed and I_a is stator current. Also, we have

$$E^2 = V^2 + (I_a \omega L_s)^2 \tag{16}$$

where V is terminal voltage of PMSG and L_s is its inductance. The rectified dc-link voltage may be obtained using

$$V_{\rm dc} = \frac{3\sqrt{6}}{\pi} V. \tag{17}$$

From (15) to (17), the rectified dc voltage may be written as

$$V_{\rm dc} = \frac{3\sqrt{6}}{\pi} \omega \sqrt{K_e^2 - \left(\frac{T L_s}{K_t}\right)^2}. \tag{18}$$

The torque is determined by the generator speed and the wind speed, therefore according to (18), it is possible to obtain a prediction for the dc voltage as a function of the generator speed and the wind speed. As result, the generator speed can be regulated by setting the dc voltage.

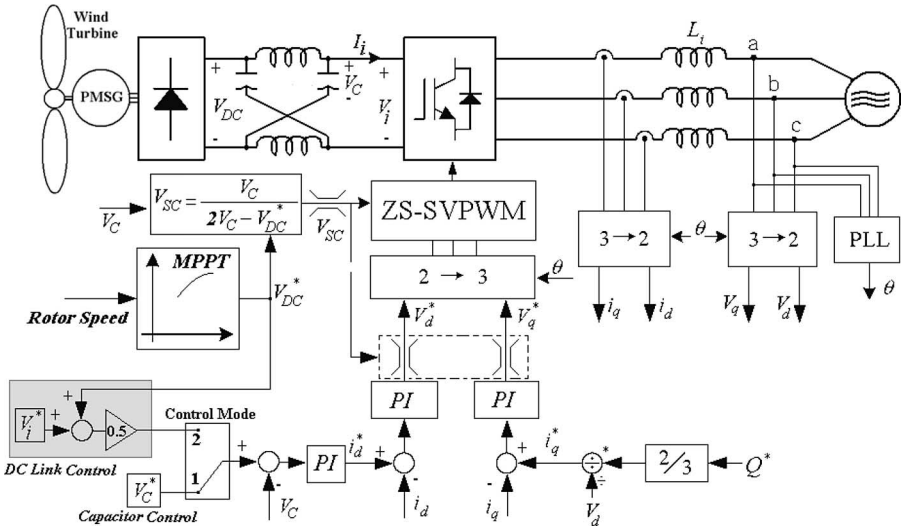

Fig. 10. Block diagram of proposed WECS control system.

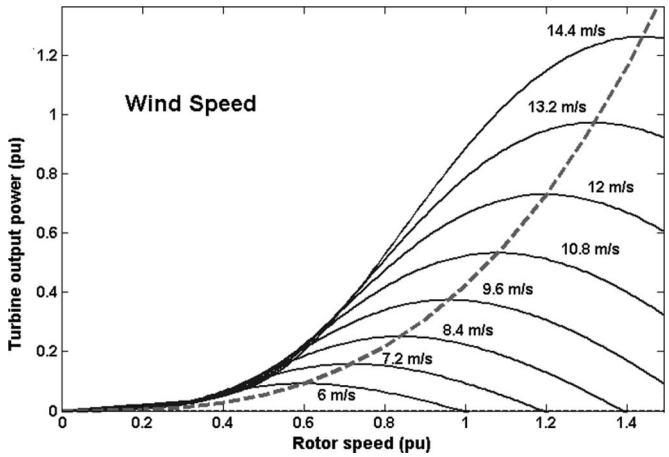

Fig. 11. Mechanical power versus rotor speed with the wind speed as a parameter.

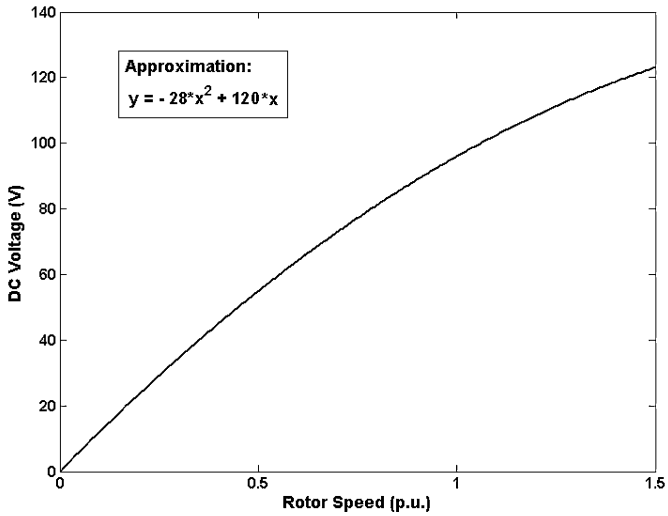

Fig. 12. DC voltage versus optimum rotor speed characteristic.

Fig. 12 shows the rectified dc voltage versus rotor speed for maximum wind power operating point. Using rotor speed feedback and Fig. 12, the optimum rectified dc voltage is specified. Using new optimum dc voltage, PMSG rotor speed will change and a new dc voltage command is specified from Fig. 12. With this control strategy, PMSG rotor speed and dc voltage is continuously changed until an equilibrium point is reached in Fig. 12 [4].

One can see from Fig. 12 that the voltage–speed relationship is not a straight line. In order to implement as simple a control strategy as possible, it is desirable to implement a straight line voltage–speed relationship. In this paper, a quadratic approximation of the voltage–speed relationship is used. After determining optimum dc voltage from voltage–speed curve, shoot-through signal V_{SC} for PWM control is calculated by

$$V_{SC} = \frac{T_1}{T} = \frac{V_C}{2V_C - V_{\mathrm{dc-Ref}}} \tag{19}$$

TABLE I
PARAMETERS OF PMSG

Parameter	Value
R_s	0.9585 Ω
L_q	5.25 mH
L_d	5.25 mH
P	4
J	6.329 Kg.cm^2

IV. SIMULATION

To verify the performance of the proposed WECS, several simulation tests are performed. The simulated system parameters are listed in Tables I and II.

Fig. 12 is plotted using mathematical model of the turbine and PMSG. The optimum curve can also be obtained by some tests in various wind speed. Solid curve in Fig. 13 is dc voltage versus optimum rotor speed. This curve is plotted with simulation of WECS for various wind speed and rotor speed. Dotted

TABLE II
SIMULATION PARAMETERS

Parameter	Value
V_G	76 V
L_i	8 mH
L_1,L_2	2 mH
C_1,C_2	2200 uF
F_s	10 kHz

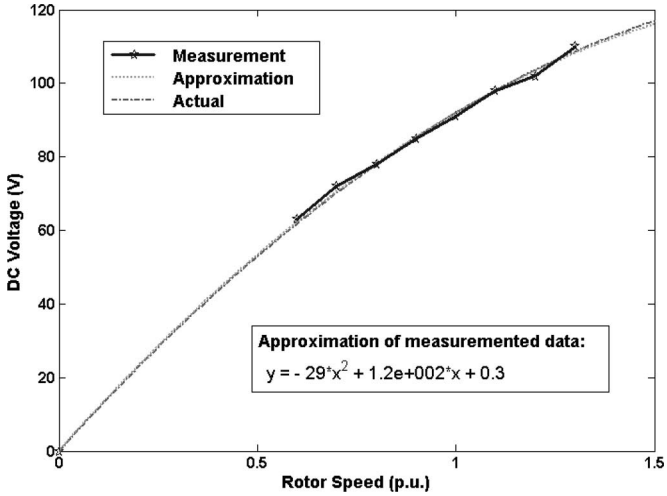

Fig. 13. DC voltage and optimum rotor speed relation: simulated and approximated and calculated (actual).

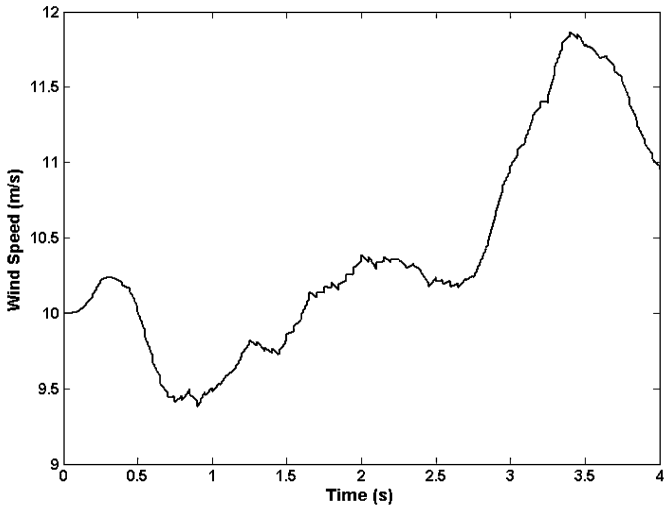

Fig. 14. Wind speed variation.

curve is a quadratic approximation of the bold curve. In next simulations, the dotted curve is used for maximum power control. The maximum and minimum rotor speeds are considered as 1.3 and 0.6 per unit (p.u.), respectively.

A. Simulation of Proposed System

In order to evaluate the dynamic performance of the proposed WECS, it is simulated for 4 s. The wind speed is shown in Fig 14. Two simulations were performed using two different methods for active power control as mentioned in Section II.

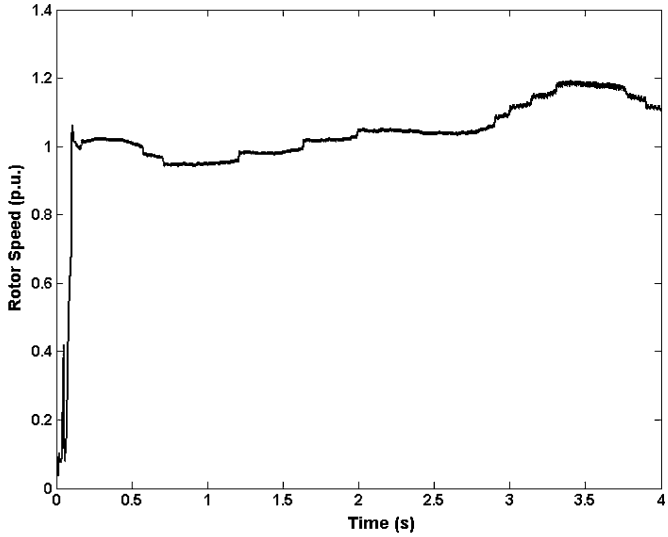

Fig. 15. PMSG rotor speed (capacitor voltage control).

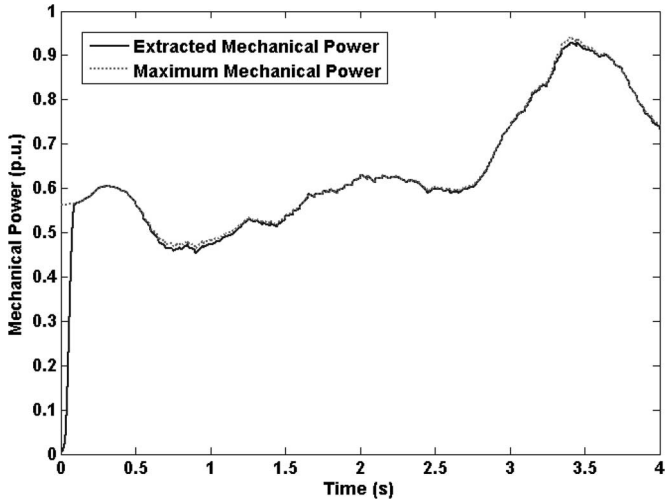

Fig. 16. Maximum mechanical power of turbine and the extracted mechanical power from turbine (capacitor voltage control).

1) Capacitor Voltage Control Method: In this section, the proposed system is simulated using capacitor voltage control of Z-source inverter. Reference voltage for capacitor was set to 140 V. Fig. 15 shows PMSG rotor speed. To obtain maximum power control, the rotor speed has changed with changing wind speed. Fig 16 shows maximum mechanical power of turbine and extracted mechanical power from turbine. It is seen that extracted mechanical power is tracking the maximum mechanical power after a short time.

Fig. 17 shows capacitor voltage, which is almost constant reactive power that is kept at zero (unity power factor) is also shown in Fig. 18.

Fig. 19 shows active power delivered to the grid and the extracted mechanical power. The electrical power delivered to the grid is different from the extracted mechanical power due to electrical and mechanical losses. Inductor current is shown in Fig. 20. It is seen that the inductor current is variable, however, current ripple is almost constant.

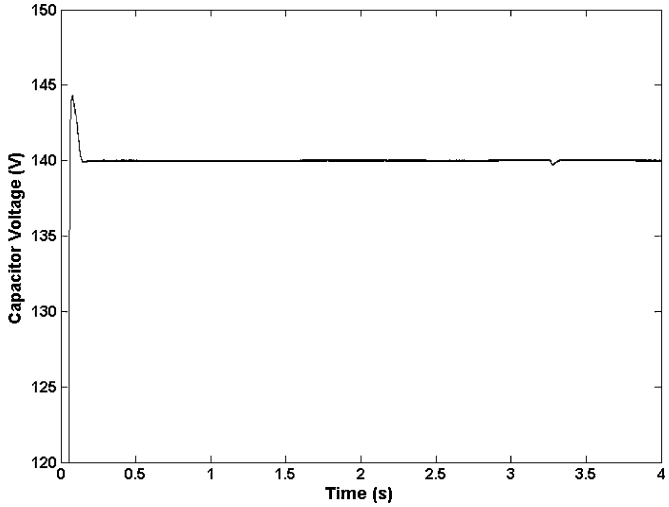

Fig. 17. Capacitor voltage (capacitor voltage control).

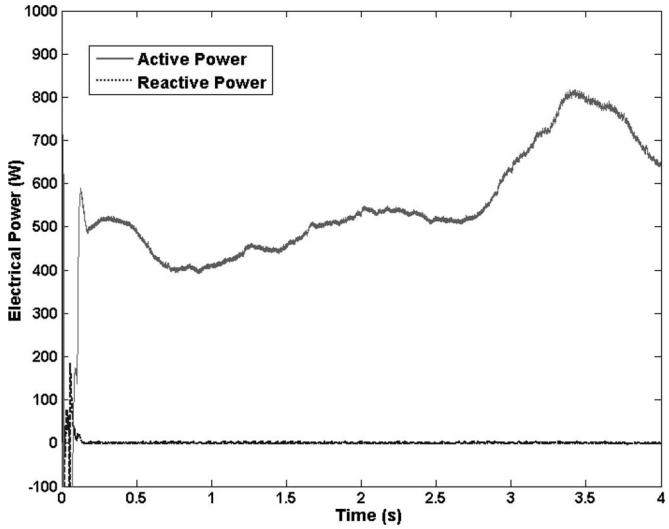

Fig. 18. Active and reactive powers (capacitor voltage control).

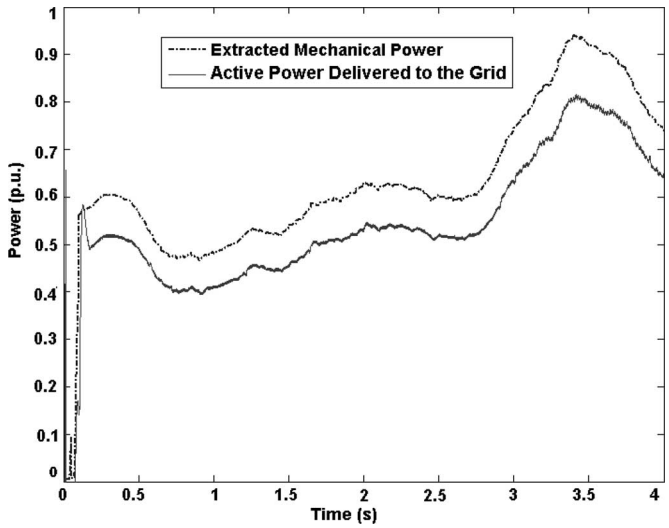

Fig. 19. Active power delivered to the grid and extracted mechanical power (capacitor voltage control).

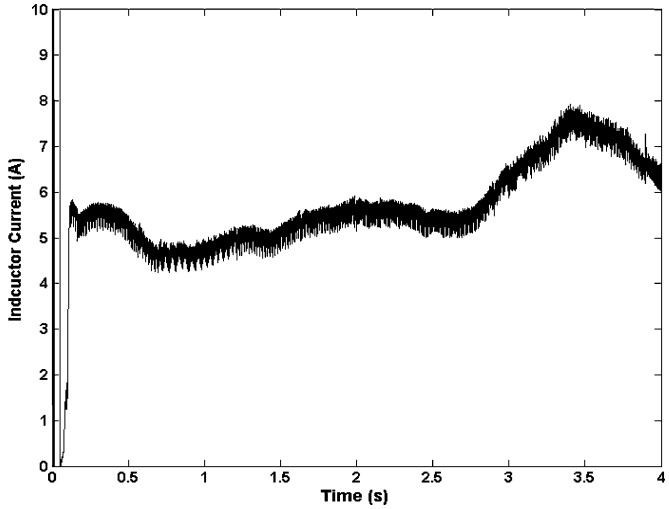

Fig. 20. Inductor current of Z-source inverter (capacitor voltage control).

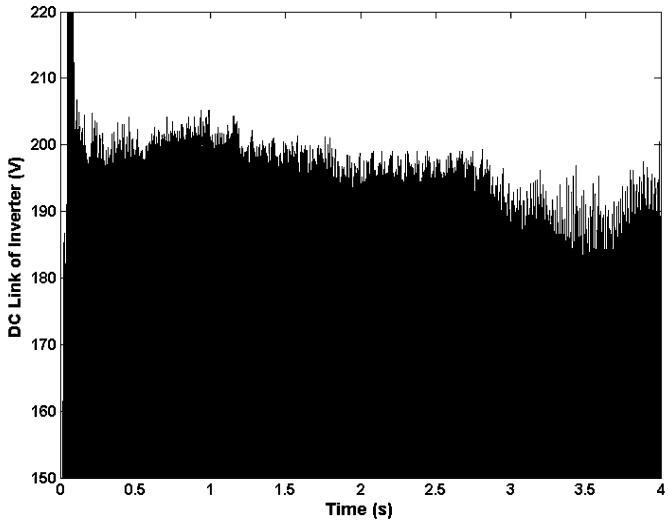

Fig. 21. Input voltage of Inverter (V_i) (capacitor voltage control).

In Fig. 21, the input voltage of inverter (V_i) is shown. For MPPT control, V_i has changed with variations of wind speed, while capacitor voltage is constant (Fig. 17) that was expected from capacitor voltage control method.

2) DC-Link Voltage Control Method: The previous simulation was repeated using dc-link voltage control. Reference voltage for dc link of Z-source inverter was set to 165 V. Figs. 22–24 show rotor speed, maximum mechanical power of turbine, the extracted mechanical power, and active power delivered to the grid. In dc-link voltage control method, for MPPT control, capacitor voltage must change, while V_i is constant, as shown in Figs. 25 and 26. The capacitor has slow dynamics. On the other hand, there is a right half-plane (RHP) zero in the transfer function of V_C, which causes undershoot in capacitor voltage [10]. However, it is not a concern for MPPT control, because dynamics of wind and turbine are slow too. We can see small undershoots in rotor speed (Fig. 22) that are not shown in Fig. 15. These undershoots have no considerable effect on MPPT, as the extracted mechanical power tracks the maximum mechanical

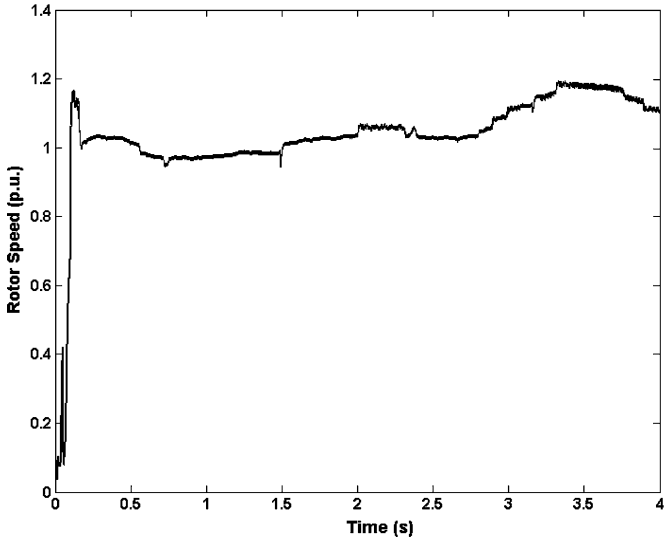

Fig. 22. PMSG rotor speed (dc-link voltage control).

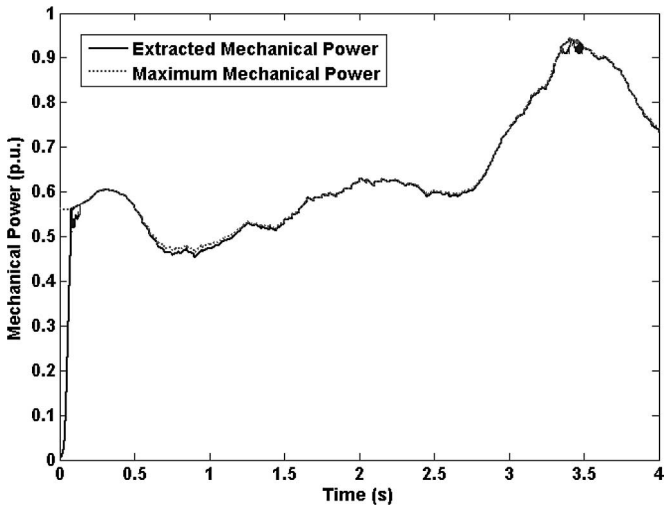

Fig. 23. The maximum mechanical power of turbine and the extracted mechanical power from turbine (dc-link voltage control).

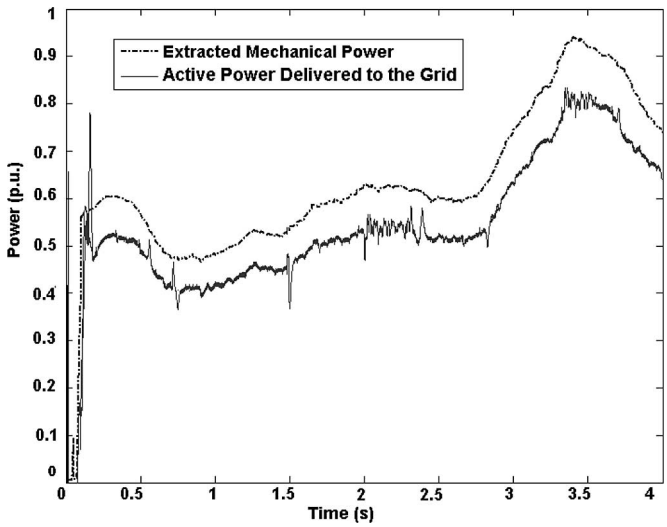

Fig. 24. Active power delivered to the grid and extracted mechanical power (dc-link voltage control).

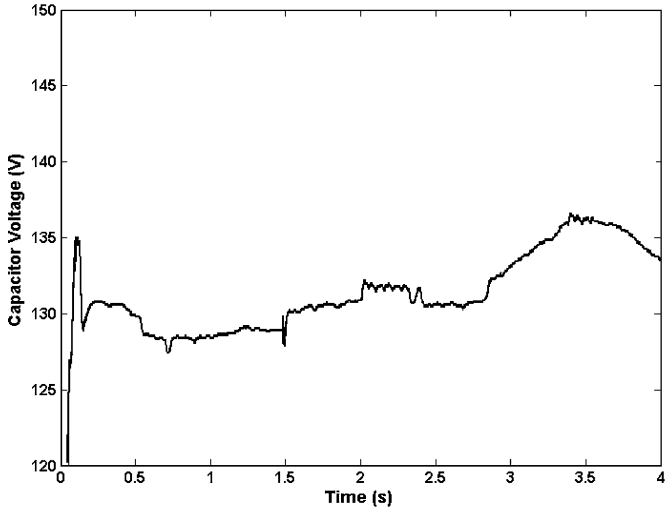

Fig. 25. Capacitor voltage (dc-link voltage control).

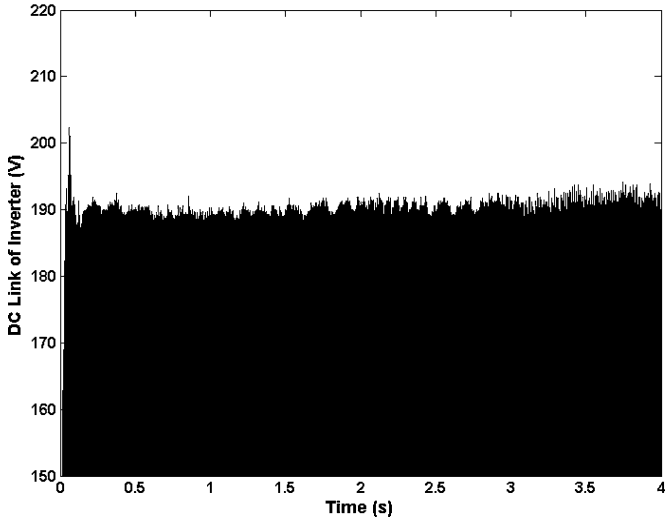

Fig. 26. Input voltage of Inverter (V_i) (dc-link voltage control).

power in Figs. 16 and 23. But variation of capacitor voltage has more effect on power delivery. As shown in Fig. 24, electrical power has more fluctuations than shown in Fig. 19.

B. Operation of Constant Wind Speed

In order to evaluate the performance of the proposed system, another simulation is performed using constant wind speed (10 m/s) and with capacitor voltage control.

Fig. 27 illustrates dc-link voltage across rectifier that is changing from 95 to 280 V. With respect to Fig. 8, when a shoot-through vector is applied to Z-source inverter, dc-link voltage of rectifier will be twice as much as the capacitor voltage (280 V). With reference to Fig. 13, when wind speed is 10 m/s, dc-link voltage across rectifier must be 95 V for MPPT. DC-link voltage across Z-source inverter is shown in Fig. 28, which is zero in shoot-through time intervals and 185 V in other times according to (6).

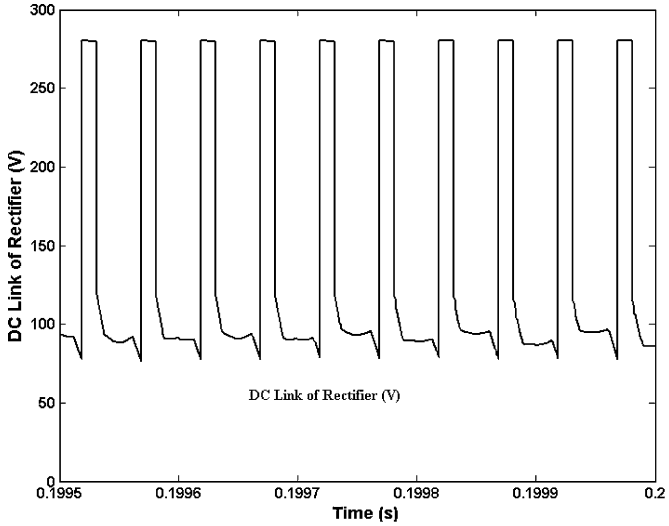

Fig. 27. DC-link voltage across the rectifier.

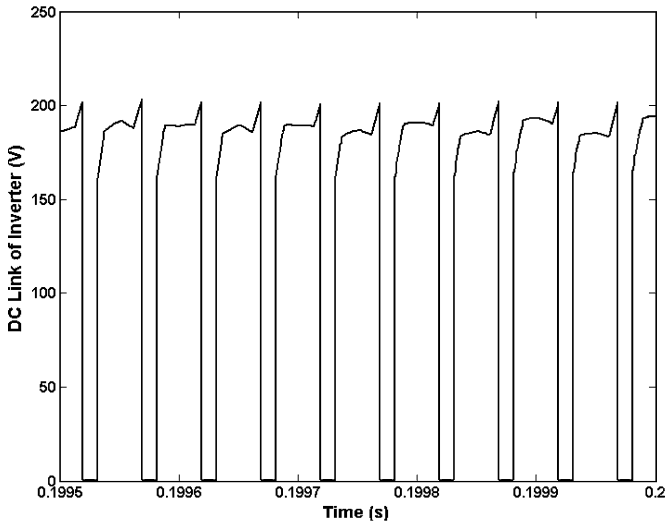

Fig. 28. DC-link voltage across the Z-source inverter.

Figs. 29 and 30 illustrate the inductor current. With respect to (7), current ripple must be 0.85 A. This is shown in Fig. 30. However, there is a low-frequency larger ripple, because Z-source inverter is fed by an uncontrolled rectifier. Figs. 31 and 32 show grid current and its spectra. THD of injected current is 2.95%.

C. Comparison With Conventional System

In this section, the proposed WECS is compared with conventional WECS using boost converter replacing the Z-source network, as shown in Fig. 1. PWM switching method is implemented to keep dc bus voltage constant that switching pulse is generated by a new control box using V_C and $V_{\rm dc}^*$. Inductance and capacitance of boost converter is selected twice as much as of the proposed system that is 4 mH and 4400 μF. To correct comparison, traditional WECS was simulated in conditions similar to previous simulation.

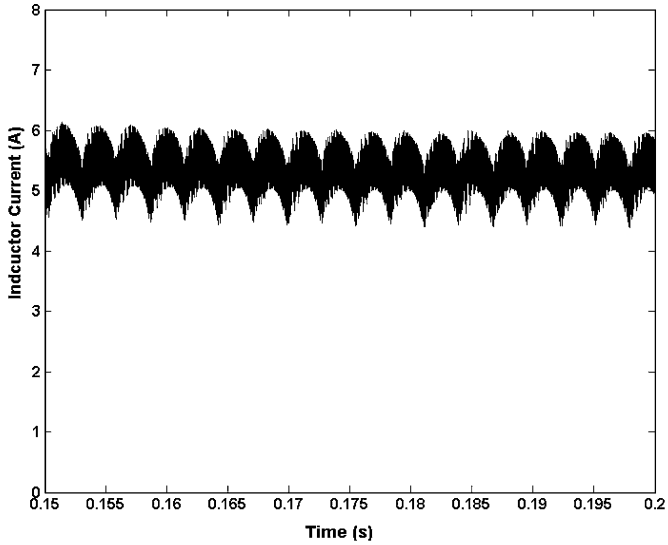

Fig. 29. Inductor current of Z-source inverter.

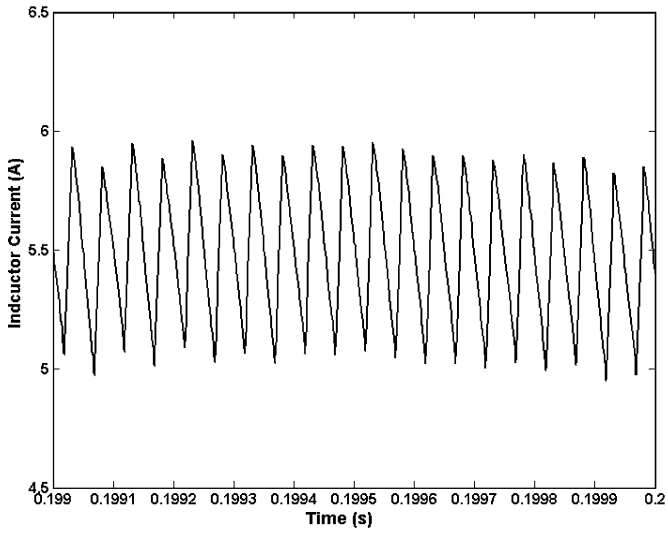

Fig. 30. Inductor current of Z-source inverter (zoomed).

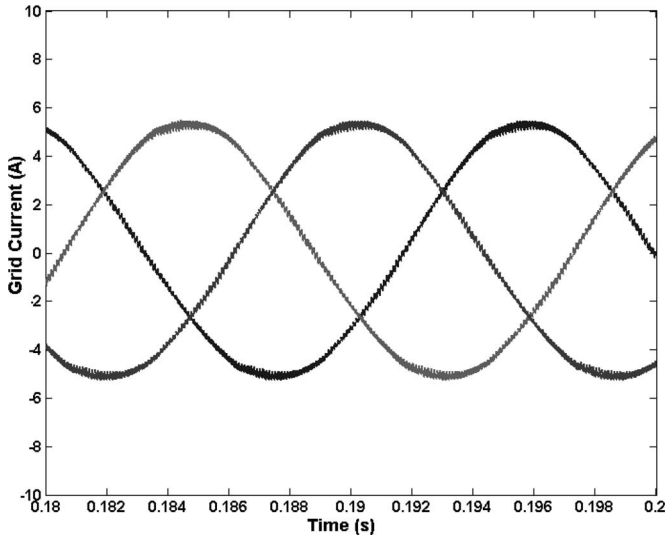

Fig. 31. Grid current in proposed WECS.

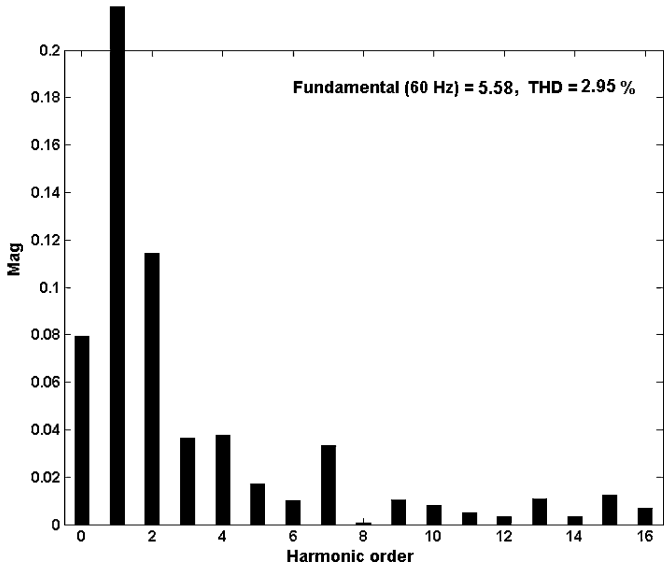

Fig. 32. Spectra of grid current in proposed WECS.

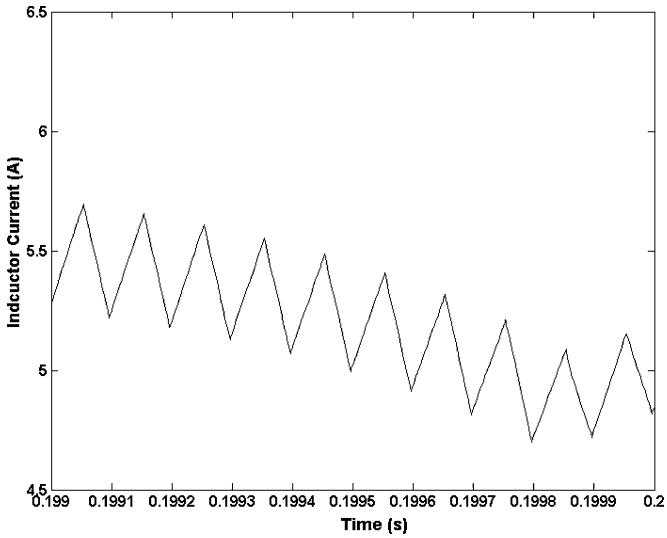

Fig. 33. Inductor current of boost converter (zoomed).

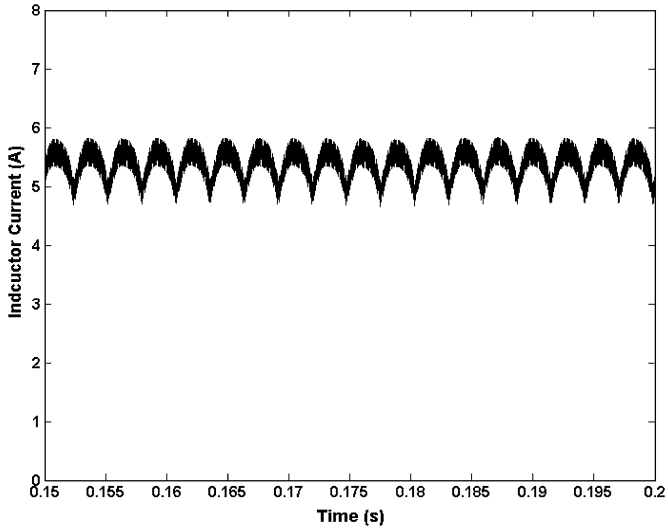

Fig. 34. Inductor current of boost converter.

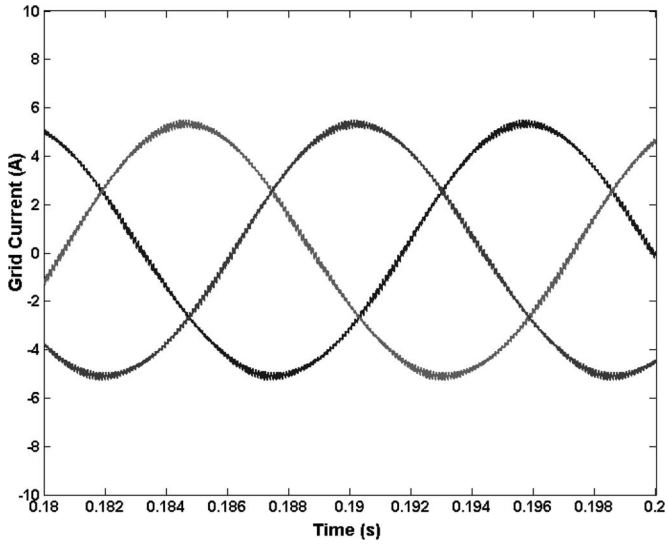

Fig. 35. Grid current in traditional WECS without dead time.

1) Inductor Current Ripple: As shown in Fig. 33, the inductor current ripple is 0.38 A as expected from theory [11]. The current ripple for the proposed WECS, as shown in Fig. 30, is twice as much that is 0.85 A. As shown in Fig. 34, there is a low-frequency ripple caused by uncontrolled rectifier. The same ripple is shown in Fig. 29 for the proposed WECS.

2) Grid Current THD: In a conventional inverter, a dead time is included in the switching of semiconductors to prevent accidental short circuit in an inverter lag. Two simulations are performed with 0 and 5 μs dead time using conventional WECS with boost converter. Figs. 35 and 36 illustrate the grid current and its spectra for zero dead time simulation. THD is 3.1% that nearly equals THD of current in proposed WECS. Figs. 37 and 38 show the grid current and its spectra for 5 μS dead time simulation. THD has increased to 4.96%.

3) Efficiency: In order to compare efficiency, both proposed and conventional WECS was simulated with various wind speeds. The active electrical power delivered to grid versus wind speed is shown in Fig. 39. In each simulation, efficiency is calculated by dividing the active electrical power by the maximum mechanical power (according to Fig. 11). Fig. 40 illustrates the efficiency of both systems in various wind speeds. According to Fig. 40, efficiency of conventional WECS is smaller than that of the proposed WECS, approximately 4%. The reason is the extra switch and diode in conventional WECS with boost converter.

4) Total Switching Device Power: The total switching device power (TSDP) is used for comparison of rating of converters in [11]. TSDP is calculated as

$$\text{TSDP} = \sum_{j=1}^{N} C_j V_{sj} I_{sj} \tag{20}$$

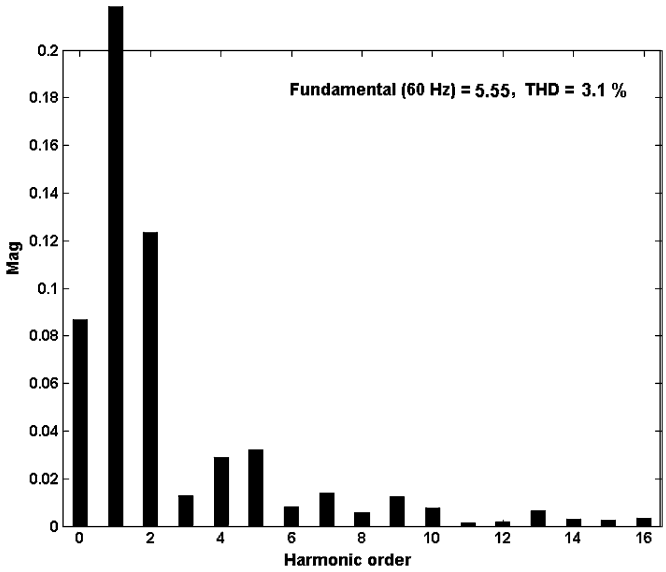

Fig. 36. Spectra of grid current in traditional WECS without dead time.

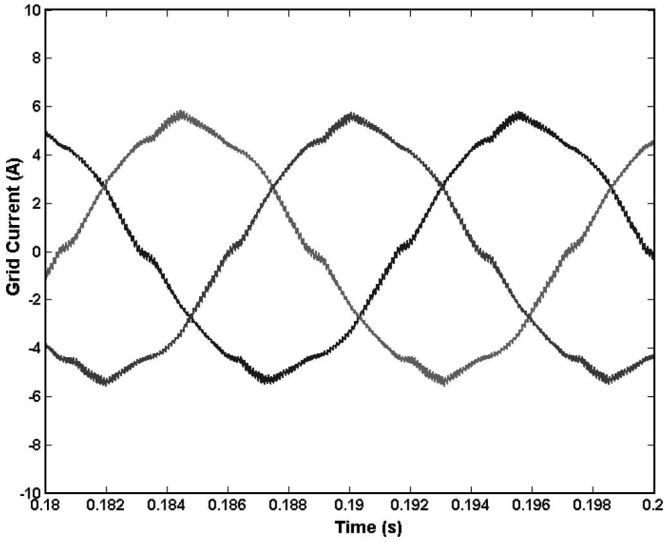

Fig. 37. Grid current in traditional WECS with dead time.

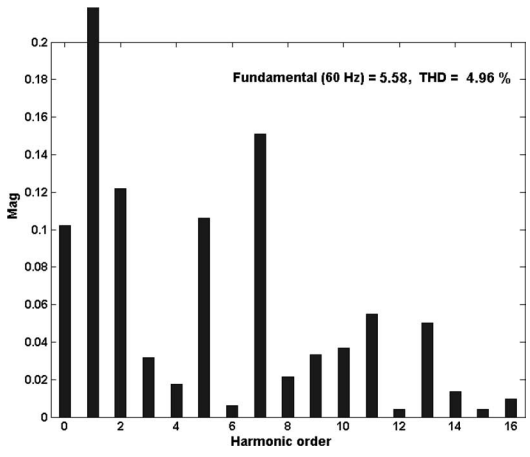

Fig. 38. Spectra of grid current in traditional WECS with dead time.

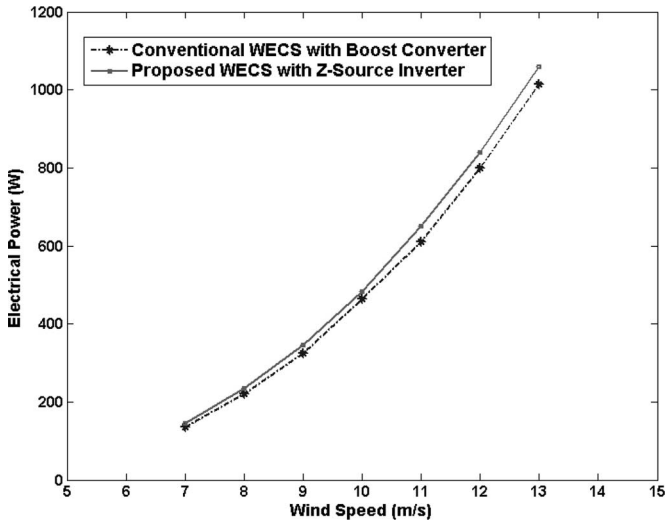

Fig. 39. Active power delivered to the grid in conventional and proposed WECSs.

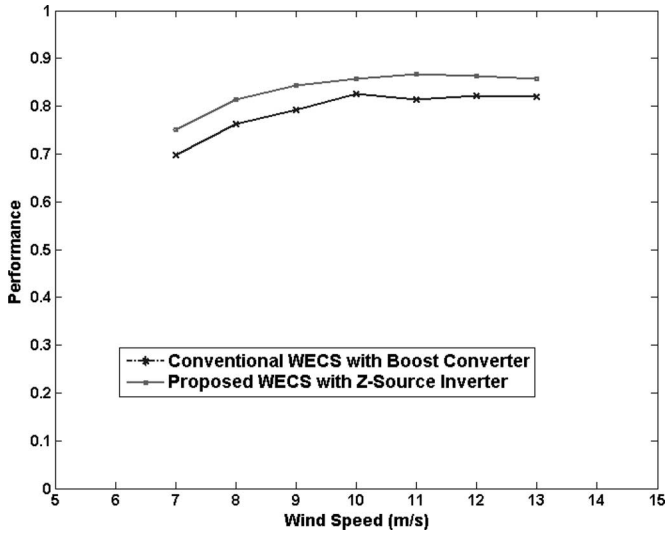

Fig. 40. Efficiency of conventional and proposed WECSs.

TABLE III
TSDP OF VARIOUS WECS

Type	*TSDP*
Conventional WECS with Boost Converter	**8482**
Proposed WECS with Capacitor Voltage Control	**10049**
Proposed WECS with DC Link Voltage Control	**9034**

where N is number of semiconductor devices, V_{sj} and I_{sj} are voltage stress and current stress of device, respectively, C_j is cost factor, and C_j is defined as 1 for semiconductor switch and 0.5 for diode.

Table III shows TSDP of WECS systems with boost converter, proposed WECS with voltage control of capacitor, and proposed WECS with voltage control of dc link. It is seen that TSDP of proposed WECS with capacitor voltage control is bigger than conventional WECS. However, with dc-link voltage capacitor, TSDP is increased only 6%.

V. Conclusion

In this paper, a PMSG-based WECS with Z-source inverter is proposed. Z-source inverter is used for maximum power tracking control and delivering power to the grid, simultaneously. Compared to conventional WECS with boost converter, the number of switching semiconductors is reduced by one and reliability of system is improved, because there is no requirement for dead time in a Z-source inverter.

For active power control, two control methods: capacitor voltage control and dc-link voltage control is proposed and compared. It is shown that with dc-link voltage control method, TSDP is increased only 6% compared to conventional system, but there is more power fluctuations compared to capacitor voltage control. With capacitor voltage control TSDP in increased 19% compared to conventional system. It was also shown that due to elimination of dead time, the THD of proposed system is reduced by 40% compared to conventional system by 5 mS dead time. Finally, with same value of passive components, inductor current ripple is the same for both systems.

References

[1] E. Spooner and A. C. Williamson, "Direct coupled permanent magnet generators for wind turbine applications," *Inst. Elect. Eng. Proc., Elect. Power Appl.*, vol. 143, no. 1, pp. 1–8, 1996.

[2] N. Yamamura, M. Ishida, and T. Hori, "A simple wind power generating system with permanent magnet type synchronous generator," in *Proc. IEEE Int. Conf. Power Electron. Drive Syst.*, 1999, vol. 2, pp. 849–854.

[3] S. H. Song, S. Kang, and N. K. Hahm, "Implementation and control of grid connected AC–DC–AC power converter for variable speed wind energy conversion system," *Appl. Power Electron. Conf. Expo.*, vol. 1, pp. 154–158, 2003.

[4] A. M. Knight and G. E. Peters, "Simple wind energy controller for an expanded operating range," *IEEE Trans. Energy Convers.*, vol. 20, no. 2, pp. 459–466, Jun. 2005.

[5] T. Tafticht, K. Agbossou, A. Cheriti, and M. L. Doumbia, "Output power maximization of a permanent magnet synchronous generator based standalone wind turbine," in *Proc. IEEE ISIE 2006*, Montreal, QC, Canada, pp. 2412–2416.

[6] M. Chinchilla, S. Arnaltes, and J. C. Burgos, "Control of permanent-magnet generators applied to variable-speed wind-energy systems connected to the grid," *IEEE Trans. Energy Convers.*, vol. 21, no. 1, pp. 130–135, Mar. 2006.

[7] F. Z. Peng, "Z-source inverter," *IEEE Trans. Ind. Appl.*, vol. 39, no. 2, pp. 504–510, Mar./Apr. 2003.

[8] F. Z. Peng, M. Shen, and Z. Qian, "Maximum boost control of the Z-source inverter," *IEEE Trans. Power Electron.*, vol. 20, no. 4, pp. 833–838, Jul. 2005.

[9] F. Z. Peng, A. Joseph, J. Wang, and M. Shen, "Z-source inverter for motor drives," *IEEE Trans. Power Electron.*, vol. 20, no. 4, pp. 857–863, Jul. 2005.

[10] P. C. Loh, D. M. Vilathgamuwa, C. J. Gajanayake, Y. R. Lim, and C. W. Teo, "Transient modeling and analysis of pulse-width modulated Z-source inverter," *IEEE Trans. Power Electron.*, vol. 22, no. 2, pp. 498–507, Mar. 2007.

[11] M. Shen, A. Joseph, J. Wang, F. Z. Peng, and D. J. Adams, "Comparison of traditional inverters and Z-source inverter," in *Proc. Power Electron. Spec. Conf.*, 2005, pp. 1692–1698.

Seyed Mohammad Dehghan (S'08) was born in Tehran, Iran, in 1981. He received the B.S. degree in electrical engineering from Azad Islamic University, Yazd, Iran, in 2003, and the M.S. degree in electrical engineering in 2005 from Tarbiat Modares University, Tehran, Iran, where he is currently working toward the Ph.D. degree.

His current research interests include inverters, motor drives, inverter-based distributed generation (DG), and flexible AC transmission systems (FACTS).

Mustafa Mohamadian (M'04) received the B.S. degree in electrical engineering from Amirkabir University of Technology, Tehran, Iran, in 1989, and the M.S. degree in electrical engineering from Tehran University, Tehran, in 1992, and the Ph.D. degree in electrical engineering, specializing in power electronics and motor drives, from the University of Calgary, Calgary, AB, Canada, in 1997.

Since 2005, he has been an Assistant Professor at the Department of Electrical and Computer Engineering, Tarbiat Modares University, Tehran. His current research interests include modeling, analysis, design, and control of power electronic converters/systems and motor drives, and embedded software development for automation, motion control, and condition monitoring of industrial systems with microcontrollers and DSPs.

Ali Yazdian Varjani (M'95) received the B.S. degree from the Sharif University of Technology, Tehran, Iran, in 1989, and the M.Eng. and Ph.D. degrees in electrical engineering from the University of Wollongong, Wollongong, N.S.W., Australia, in 1995 and 1999, respectively.

From 1988 to 1990, he was an Elec. and Comp. Engineer with Electric Power Research Centre, Tehran. From 1990 to 1992, he was an Electrical Engineer and then a Senior Engineer at Ministry of Energy where he gained considerable industrial experience primarily in computer and power systems engineering. From 1999 to 2000, he was the Technical Manager of Iran University Network project in Iranian Research Organization for Science and Technology (IROST). From 2001 to 2004, he was a senior consultant engaged in strategic planning for Information and Communication Technology (ICT) development in Iran Telecom Research Centre (ITRC). Since 1999, he has been an Assistant Professor at the Department of Electrical and Computer Engineering, Tarbiat Modares University, Tehran. His current research interests include DSP applicable in harmonics (power quality) and power-electronics-based drive systems, and a variety of research issues associated with the "information and communication technology" including internet-enabled services, ad hoc networking, and network security and control.